Journal of Fractional Calculus and Applications
Vol. 12(1) Jan. 2021, pp. 9-24.
ISSN: 2090-5858.
http://math-frac.oreg/Journals/JFCA/

PATTERN FORMATION IN A TIME FRACTIONAL REACTION-DIFFUSION SYSTEM

L. W. SOMATHILAKE , K. BURRAGE

ABSTRACT. The main, aim of this paper is to analyse spatial temporal pattern formation behaviour of a time fractional reaction-diffusion system (TFRDS). In order to identify this behaviour, we perform a Turing instability analysis and determine the parameter regions of the model in which the Turing instability occur (the Turing instability space). We discuss the effects of the time fractional order and the model parameters on the spatial temporal pattern formation in the model. Next, we solve the considered TFRDS using a finite difference scheme of solving time fractional differential equations (TFDEs). In order to apply this finite difference scheme we transform the TFRDS in to a system of TFDEs by discretising in space. We solved this system of TFDEs using an Implicit Finite difference scheme. We observed that the numerical solutions agree with pattern formation properties shown via the instability analysis of the model.

1. INTRODUCTION

The purpose of this investigation is to explore the suitability of time fractional phenomena in pattern formations in a reaction diffusion model. Fractional differential equations and fractional reaction diffusion equations (FRDEs) of various types play important roles in many application areas such as engineering, physics, control systems, dynamical systems, finance, and are often associated with anomalous diffusion and Levy flight behaviours.

The general form of the one variable time-fractional standard-diffusion reaction equation is:

$$\frac{\partial^\gamma u}{\partial t^\gamma} = D\Delta u + f(u,t). \tag{1.1}$$

Here D and $f(u,t)$ represent the diffusion rate and source term respectively and $\dfrac{\partial^\gamma}{\partial t^\gamma}$ is the time fractional derivative operator. The fractional derivative of a function can be defined in different ways including the Caputo fractional derivative and Riemann-Liouville fractional derivative [1].

Finding analytical solutions of nonlinear fractional reaction diffusion equations arising in modelling physical phenomena is very difficult or impossible. In such cases numerical techniques play an important role in finding approximate solutions. In the literature

---

2010 *Mathematics Subject Classification.* 26A33, 35R11, 35B36, 70K50.
Key words and phrases. Time Fractional-Reaction-Diffusion Equations, Instability Analysis, Pattern formations, Fractional-Order Derivatives.
Submitted Dec. 5, 2019. Revised Jan. 17, 2020.

a number of authors have developed numerical methods for fractional reaction diffusion equations [2, 3, 4, 5, 6, 7, 8, 9, 10, 11, 18, 19, 12, 13].

Performing a linear instability analysis of FRDEs is helpful to identify their spatial temporal pattern formation behaviour. Instability analysis and pattern formation behaviour of time fractional reaction diffusion equations are given in [14, 15, 16]. In this paper, we propose a time fractional-reaction-diffusion system (TFRDS) based on the space fractional reaction-diffusion model proposed in [17] and the spatial temporal pattern formation behaviour of the proposed model is investigated. The results of analytical treatments of the instabilities of the model are validated by computer simulations of the model.

The paper is organized as follows. A time fractional reaction diffusion model based on space fractional RDS reported in [17] is introduced in section 1.1. Numerical methods for time fractional differential equations are explained in section 2.1. A Turing type instability analysis of the TFRDS is given in section 2.2. Also, in the same section, the effects of the time fractional exponent on growth and spatial temporal pattern formation by the solutions of the model are analysed. In section 3.3, numerical results on one and two dimensions are presented. Finally, discussion and conclusion based on the results are presented in section 4.

1.1. **Mathematical model.** In [17] a Space-Fractional Reaction-Diffusion model for growth of coral in a tank is proposed in the form

$$\begin{aligned}
\frac{\partial u}{\partial t} &= -d_u(-\Delta)^{\alpha/2}u + b(u_s - u) - b_1 v^2 u \\
\frac{\partial v}{\partial t} &= -d_v(-\Delta)^{\alpha/2}v - b_2 v + b_1 v^2 u \qquad (1.2)\\
\frac{\partial w}{\partial t} &= b_2 v.
\end{aligned}$$

Here u and v denote the biomasses of dissolved nutrients of polyps and dissolved solid material (calcium carbonate ions) in the tank, respectively and w denotes the biomass of depositing amount of solid materials on the existing corals. In addition, d_u and d_v denote the diffusion rates of u and v, respectively, and b and b_2 denote the nutrient supplying rate to the system and depositing rate of v, respectively. b_1 is the reaction rate between nutrients and polyps. Here $\alpha > 1$ is the fractional exponent of the spatial diffusion operator of u and v. Also, $u_s = a/b$ and $b(u - u_s)$ is the overall nutrient supply rate to the system. In the case of standard diffusion $\alpha = 2$ the corresponding time fractional model can be written in the form

$$\begin{aligned}
\frac{\partial^\gamma u}{\partial t^\gamma} &= d_u \Delta u + b(u_s - u) - b_1 v^2 u \\
\frac{\partial^\gamma v}{\partial t^\gamma} &= d_v \Delta v - b_2 v + b_1 v^2 u \qquad (1.3)\\
\frac{\partial w}{\partial t} &= b_2 v.
\end{aligned}$$

In order to reduce the number of parameters, we use nondimensionalisation techniques.

1.1.1. *Nondimensionalisation.* Now we nondimensionalise the proposed model by applying the coordinate transformations $t^* = b^{1/\gamma}t$, $x^* = \frac{x}{L}$, $y^* = \frac{y}{L}$, $z^* = \frac{z}{L}$, where $L = (d_u/b)^{1/2}$ giving

$$
\begin{aligned}
\frac{\partial^\gamma \bar{u}}{\partial t^{*\gamma}} &= \Delta^* \bar{u} + 1 - \bar{u} - \alpha^2 \bar{v}^2 \bar{u} \\
\frac{\partial^\gamma \bar{v}}{\partial t^{*\gamma}} &= d\Delta^* \bar{v} - \lambda \bar{v} + \alpha^2 \bar{v}^2 \bar{u} \\
\frac{\partial \bar{w}}{\partial t^*} &= \lambda \bar{v},
\end{aligned}
\tag{1.4}
$$

where $\bar{u} = \dfrac{u}{u_s}$, $\bar{v} = \dfrac{v}{u_s}$, $\alpha^2 = \dfrac{b_1 u_s^2}{b}$ and $\lambda = \dfrac{b_2}{b}$, $d = \dfrac{d_v}{d_u}$.

For notational convenience, eliminating *bars* and *stars* we obtain

$$
\begin{aligned}
\frac{\partial^\gamma u}{\partial t^\gamma} &= \Delta u + 1 - u - \alpha^2 u v^2 \\
\frac{\partial^\gamma v}{\partial t^\gamma} &= d\Delta v - \lambda v + \alpha^2 u v^2 \\
\frac{\partial w}{\partial t} &= \lambda v.
\end{aligned}
\tag{1.5}
$$

In this system, first two equations are independent of w. Therefore, only first two equations were considered in analysis and numerical simulations of this paper. Just after finding numerical solutions of first two equations, the numerical solution for w can be calculated by substituting v-solution into third equation of this system. But, in this paper we didn't concern on the solutions for w. The time derivative of the third equation of the system can be considered as fractional derivative or non-fractional partial derivative.

1.1.2. *Boundary conditions.* In this paper we consider homogeneous Neumann boundary conditions:

$$
\left.
\begin{array}{ll}
\nabla u.\mathbf{n} = 0, & x \in \partial\Omega \\
\nabla v.\mathbf{n} = 0, & x \in \partial\Omega
\end{array}
\right\},
\tag{1.6}
$$

where Ω is the considered domain and $\mathbf{n}$ denotes the outwards unit normal vector to the boundary $\partial\Omega$.

2. Methodology

2.1. **Numerical Methods.**

2.1.1. *Space discretisation.* Now we represent the first two equations of the system (1.5) in the form:

$$
\begin{aligned}
\frac{\partial^\gamma u}{\partial t^\gamma} &= \Delta u + \overbrace{(1 - u - \alpha^2 u v^2)}^{F(u,v)}, \\
\frac{\partial^\gamma v}{\partial t^\gamma} &= d\Delta v + \overbrace{(-\lambda v + \alpha^2 u v^2)}^{G(u,v)}.
\end{aligned}
\tag{2.7}
$$

Discretising in space, time fractional reaction diffusion system (2.7) can be approximated by a system of ODEs on the bounded domain Ω as follows:

$$\begin{aligned} \frac{d^\gamma \mathbf{u}}{dt^\gamma} &= -\frac{1}{h^2}A\mathbf{u} + \mathbf{F}(\mathbf{u},\mathbf{v}), \quad t \in [0,T] \\ \frac{d^\gamma \mathbf{v}}{dt^\gamma} &= -\frac{d}{h^2}A\mathbf{v} + \mathbf{G}(\mathbf{u},\mathbf{v}), \quad t \in [0,T]. \end{aligned} \tag{2.8}$$

Here $\frac{-1}{h^2}A$ is the discrete Laplace operator coupled with the boundary condition (1.6). The vectors $\mathbf{u}$, $\mathbf{v}$, $\mathbf{F}$ and $\mathbf{G}$ represent the spatial discretisations of u, v, $F(u,v)$ and $G(u,v)$, respectively. The discrete Laplace operator, A, on $[0,L]$ coupled with homogeneous Neumann boundary conditions, obtained with a finite difference approximation on a uniform mesh of $n+1$ nodes with step size $h = L/n$ is given by

$$A = \begin{pmatrix} 2 & -2 & & & \\ -1 & 2 & -1 & & \\ & \ddots & \ddots & \ddots & \\ & & -1 & 2 & -1 \\ & & & -2 & 2 \end{pmatrix}_{(n+1)\times(n+1)}. \tag{2.9}$$

Let A_1, A_2 and A be the discrete Laplace operators on $[0,L_1]$, $[0,L_2]$ and $[0,L_1]\times[0,L_2]$, respectively. Boundary conditions embedded on A_1, A_2 and A should coincide. Then, in the usual notation, $A = A_1 \otimes I_y + I_x \otimes A_2$, where I_x and I_y are the identity matrices whose sizes are sizes of A_1 and A_2, respectively.

2.1.2. *A Finite difference scheme.* Discretizing the time fractional Caputo derivative of order γ $(0<\gamma<1)$, by the finite difference formula of first order [20] we get:

$$\frac{d^\gamma u(t_m)}{dt^\gamma} = {}_0D_{t_m}^{\ \gamma} u(t) = \frac{1}{(\Delta t)^\gamma} \sum_{k=0}^{m=\lceil t/\Delta t\rceil} g_k^\gamma (u^{m-k} - u^0), \tag{2.10}$$

where $\lceil x \rceil$ denotes the largest integer less than or equal to a real number x and u^n denotes the numerical approximation to the exact value $u(t_n)$, $t_n = n\Delta t$ for $n = 1,2,3,....$ Here, $g_k^\gamma = (-1)^k \begin{pmatrix} \gamma \\ k \end{pmatrix}$ where $\begin{pmatrix} \gamma \\ k \end{pmatrix} = \frac{\Gamma(\gamma+1)}{k!\Gamma(\gamma-k+1)}$ represents the fractional binomial coefficients.

In addition, g_k^γ satisfy the recursive relation $g_0^\gamma = 1$, $g_k^\gamma = \left(1 - \frac{\gamma+1}{k}\right) g_{k-1}^\gamma$ for $k > 1$. Now we discretize the time fractional derivative of order γ of (2.8), using the above finite difference formula.

$$\begin{aligned} \frac{1}{(\Delta t)^{(\gamma)}} \sum_{k=0}^{m} g_k^\gamma (\mathbf{u}^{(m-k)} - \mathbf{u}^0) &= -\frac{1}{h^2}A\mathbf{u}^m + \mathbf{F}^m, \\ \frac{1}{(\Delta t)^{(\gamma)}} \sum_{k=0}^{m} g_k^\gamma (\mathbf{v}^{(m-k)} - \mathbf{v}^0) &= -\frac{d}{h^2}A\mathbf{v}^m + \mathbf{G}^m. \end{aligned} \tag{2.11}$$

Here $\mathbf{u}^m = \mathbf{u}(t_m)$, $\mathbf{v}^m = \mathbf{v}(t_m)$, $\mathbf{F}^m = \mathbf{F}(\mathbf{u}_m, \mathbf{v}_m)$ and $\mathbf{G}^m = \mathbf{G}(\mathbf{u}_m, \mathbf{v}_m)$ This system can be rearranged to the following implicit system of equations:

$$\begin{aligned} \left(I + \frac{(\Delta t)^\gamma}{h^2} A\right) \mathbf{u}^m &= \mathbf{u}^0 - \sum_{k=1}^{m} g_k^\gamma \left(\mathbf{u}^{(m-k)} - \mathbf{u}^0\right) + (\Delta t)^\gamma \mathbf{F}^m, \\ \left(I + \frac{(\Delta t)^\gamma}{h^2} A\right) \mathbf{v}^m &= \mathbf{v}^0 - \sum_{k=1}^{m} g_k^\gamma \left(\mathbf{v}^{(m-k)} - \mathbf{v}^0\right) + (\Delta t)^\gamma \mathbf{G}^m. \end{aligned} \tag{2.12}$$

In order to solve this implicit system of equations, we use following iterative process

$$\begin{aligned} \left(I + \frac{(\Delta t)^\gamma}{h^2} A\right) \mathbf{u}^{m,p+1} &= \mathbf{u}^0 - \sum_{k=1}^{m} g_k^\gamma \left(\mathbf{u}^{(m-k)} - \mathbf{u}^0\right) + (\Delta t)^\gamma \mathbf{F}^{m,p}, \\ \left(I + \frac{(\Delta t)^\gamma}{h^2} A\right) \mathbf{v}^{m,p+1} &= \mathbf{v}^0 - \sum_{k=1}^{m} g_k^\gamma \left(\mathbf{v}^{(m-k)} - \mathbf{v}^0\right) + (\Delta t)^\gamma \mathbf{G}^{m,p} \end{aligned} \tag{2.13}$$

for $p = 0, 1, 2, ..., M$. Here $\mathbf{u}^{m,0} = \mathbf{u}^m$, $\mathbf{v}^{m,0} = \mathbf{v}^m$ for $m = 1, 2, ..., n$ and M is an integer suitably chosen to converge the iterative process. In each time step the iterative process proceeds until the relative error (RE) becomes smaller than the predefined tolerance (`Tol`). M is determined as the termination point of this process. The relative error RE^{m,p} at iteration p at time step m is calculated as follows:

$$\text{RE}^{m,p} = \max\left\{\frac{||\mathbf{u}^{m,p} - \mathbf{u}^{m,p-1}||}{||\mathbf{u}^{m-1}||}, \frac{||\mathbf{v}^{m,p} - \mathbf{v}^{m,p-1}||}{||\mathbf{v}^{m-1}||}\right\}. \tag{2.14}$$

The tolerance is set as $\texttt{Tol} = 10^{-13}$ in the simulations of this paper.

2.2. **Instability of the model.**
Steady states: There are three homogeneous steady states $S_1 \equiv (u_{s1}, v_{s1})$, $S_2 \equiv (u_{s2}, v_{s2})$ and $S_3 \equiv (u_{s3}, v_{s3})$ for the corresponding system of ordinary differential equations. Here $u_{s1} = 1$, $v_{s1} = 0$, $u_{s2} = \dfrac{\alpha - \sqrt{\alpha^2 - 4\lambda^2}}{2\alpha}$, $v_{s2} = \dfrac{\alpha + \sqrt{\alpha^2 - 4\lambda^2}}{2\alpha\lambda}$, $u_{s3} = \dfrac{\alpha + \sqrt{\alpha^2 - 4\lambda^2}}{2\alpha}$ and $v_{s3} = \dfrac{\alpha - \sqrt{\alpha^2 - 4\lambda^2}}{2\alpha\lambda}$ for $\alpha > 2\lambda$.

The trivial steady state S_1 is a stable node, S_3 is a saddle point and the stability of S_2 further depends on the values of the parameters α and λ. Therefore, Turing type instability may occur only at S_2. Now we derive Turing type instability conditions for the system (2.7).

By linearising (2.7) about a steady state (u_{s2}, v_{s2}) we get

$$\frac{\partial^\gamma u_1}{\partial t^\gamma} = \Delta u_1 + F_u(u_{s2}, v_{s2})u_1 + F_v(u_{s2}, v_{s2})v_1,$$

$$\frac{\partial^\gamma v_1}{\partial t^\gamma} = d\Delta v_1 + G_u(u_{s2}, v_{s2})u_1 + G_v(u_{s2}, v_{s2})v_1,$$

where u_1 and v_1 are small perturbations of (u_{s2}, v_{s2}) such that $u = u_{s2} + u_1$ and $v = v_{s2} + v_1$. This system can be written in the form

$$\begin{aligned} \frac{\partial^\gamma u_1}{\partial t^\gamma} &= \Delta u_1 + a_{11} u_1 + a_{12} v_1, \\ \frac{\partial^\gamma v_1}{\partial t^\gamma} &= d\Delta v_1 + a_{21} u_1 + a_{22} v_1, \end{aligned} \tag{2.15}$$

where $a_{11} = F_u(u_{s2}, v_{s2})$, $a_{12} = F_v(u_{s2}, v_{s2})$, $a_{21} = G_u(u_{s2}, v_{s2})$ and $a_{22} = G_v(u_{s2}, v_{s2})$. Taking the spatial Fourier transform we obtain

$$\begin{aligned} \frac{d^\gamma}{dt^\gamma} \tilde{u}_1(k,t) &= -k^2 \tilde{u}_1(k,t) + a_{11} \tilde{u}_1(k,t) + a_{12} \tilde{v}_1(k,t), \\ \frac{d^\gamma}{dt^\gamma} \tilde{v}_1(k,t) &= -dk^2 \tilde{v}_1(k,t) + a_{21} \tilde{u}_1(k,t) + a_{22} \tilde{v}_1(k,t), \end{aligned} \tag{2.16}$$

where $\tilde{u}_1(k,t)$ and $\tilde{v}_1(k,t)$ denote the spatial Fourier transforms of $u(x,t)$ and $v(x,t)$, respectively. Now taking the temporal Laplace transform we obtain

$$\begin{aligned} \sigma^\gamma \hat{\tilde{u}}_1(k,\sigma) - \tilde{u}_1(k,0) &= -k^2 \hat{\tilde{u}}_1(k,\sigma) + a_{11} \hat{\tilde{u}}_1(k,\sigma) + a_{12} \hat{\tilde{v}}(k,\sigma), \\ \sigma^\gamma \hat{\tilde{v}}_1(k,\sigma) - \tilde{v}_1(k,0) &= -dk^2 \hat{\tilde{v}}_1(k,s) + a_{21} \hat{\tilde{u}}_1(k,\sigma) + a_{22} \hat{\tilde{v}}_1(k,\sigma), \end{aligned} \tag{2.17}$$

where $\hat{\tilde{u}}_1(k,\sigma)$ and $\hat{\tilde{v}}_1(k,\sigma)$ denote the temporal Laplace transforms of $\tilde{u}_1(k,t)$ and $\tilde{v}_1(k,t)$, respectively. This system can be written in the form

$$\begin{pmatrix} \sigma^\gamma + k^2 - a_{11} & -a_{12} \\ -a_{21} & \sigma^\gamma + dk^2 - a_{22} \end{pmatrix} \begin{pmatrix} \hat{\tilde{u}}_1(k,\sigma) \\ \hat{\tilde{v}}_1(k,\sigma) \end{pmatrix} = \begin{pmatrix} \tilde{u}_1(k,0) \\ \tilde{v}_1(k,0) \end{pmatrix}. \tag{2.18}$$

Solving this system we get $\hat{\tilde{u}}_1(k,\sigma) = \dfrac{P(\sigma,k)}{R(\sigma,k)}$, $\hat{\tilde{v}}_1(k,\sigma) = \dfrac{Q(\sigma,k)}{R(\sigma,k)}$, where
$P(\sigma,k) = (\sigma^\gamma + k^2 - a_{11})\tilde{u}_1(k,0) + a_{12}\tilde{v}_1(k,0)$,
$Q(\sigma,k) = (\sigma^\gamma + dk^2 - a_{22})\tilde{v}_1(k,0) + a_{21}\tilde{u}_1(k,0)$ and
$R(\sigma,k) = (\sigma^\gamma + k^2 - a_{11})(\sigma^\gamma + dk^2 - a_{22}) - a_{12}a_{21}$.
The denominator $R(\sigma,k)$ can be written in the form

$$R(\sigma,k) = s^2 - g(\mu)s + h(\mu). \tag{2.19}$$

Here $s = \sigma^\gamma$, $\mu = k^2$, $g(\mu) = a_{11} + a_{22} - \mu - d\mu$ and $h(\mu) = d\mu^2 - (da_{11} + a_{22})\mu + a_{11}a_{22} - a_{12}a_{21}$. In terms of the model parameters

$$\begin{aligned} g(\mu) &= \frac{\left(\alpha^2 - 2\lambda^3 + \alpha\sqrt{\alpha^2 - 4\lambda^2} + 2\lambda^2\mu + 2d\lambda^2\mu\right)}{2\lambda^2}, \\ h(\mu) &= \frac{\alpha^2\,(\lambda + d\mu) + \alpha\sqrt{\alpha^2 - 4\lambda^2}\,(\lambda + d\mu) - 2\lambda^2\left(-d\mu^2 + \lambda\,(2+\mu)\right)}{2\lambda^2}. \end{aligned}$$

Let $s \equiv s_1(\mu)$ and $s \equiv s_2(\mu)$ be the solutions of the equation $R(\sigma,k) = s^2 - g(\mu)s + h(\mu) = 0$. Then we have
$\hat{\tilde{u}}_1(\mu,\sigma) = \dfrac{A_1}{s - s_1} + \dfrac{B_1}{s - s_2}$, $\hat{\tilde{v}}_1(\mu,\sigma) = \dfrac{C_1}{s - s_1} + \dfrac{D_1}{s - s_2}$, where $A_1 = \dfrac{P(s_1,\mu)}{s_1 - s_2}$,
$B_1 = \dfrac{-P(s_2,\mu)}{s_1 - s_2}$, $C_1 = \dfrac{Q(s_1,\mu)}{s_1 - s_2}$, $D_1 = \dfrac{-Q(s_2,\mu)}{s_1 - s_2}$.
Taking the inverse Laplace transform of $\hat{\tilde{u}}_1(k,\sigma)$ and $\hat{\tilde{v}}_1(k,\sigma)$ we find
$\tilde{u}_1 = A_1 E_\gamma(s_1 t^\gamma) + B_1 E_\gamma(s_2 t^\gamma)$ and $\tilde{v}_1 = C_1 E_\gamma(s_1 t^\gamma) + D_1 E_\gamma(s_2 t^\gamma)$,

where $E_{\gamma}(z)=\sum_{k=0}^{\infty}\frac{z^k}{\Gamma(k\gamma+1)}$ is the Mittag-Leffler function, Γ is the gamma function. If $s_1(\mu)$ or $s_2(\mu)$ is positive for some values of μ then the perturbation, involving those s_1 or s_2 will grow with time and Turing patterns will form. Now we derive conditions for such Turing patterns to exist.

In order for Turing instability at S_2 to exist, this steady state should be stable in the absent of diffusion. For this the conditions $C_1 \equiv a_{11}a_{22}-a_{12}a_{21}>0$, $C_2 \equiv a_{11}+a_{22}<0$ should be satisfied. Therefore, a positive real solution for s in equation (2.19) exist only if $h(\mu)<0$. Now we find the critical values of $h(\mu)$.
$\frac{dh(\mu)}{d\mu}=2d\mu-(da_{11}+a_{22})$
$\frac{dh(\mu)}{d\mu}=0 \Rightarrow 2d\mu-(da_{11}+a_{22})=0 \Rightarrow \mu=\mu_c=k_c^2=\frac{da_{11}+a_{22}}{2d}$.
Then $h(\mu)$ has a single minimum,
$h_{\text{min}}(\mu)=\frac{4d(a_{11}a_{22}-a_{12}a_{21})-(da_{11}+a_{22})^2}{4d}$, at $\mu=\mu_c=k_c^2$. Therefore, the condition $h_{\text{min}}=h(\mu_c)<0$ is satisfied if the conditions:
$C_3 \equiv\ da_{11}+a_{22}>0$ and $C_4 \equiv 4d(Det(A))-(da_{11}+a_{22})^2<0$ are satisfied. That is if the conditions C_1 to C_4 are satisfied, then there exist real roots $s_{1,2}(\alpha,\lambda,d,\mu)=\frac{g(\mu)\pm\sqrt{(g(\mu))^2-h(\mu)}}{2}$ for (2.19) such that $s_1>0$ and $s_2<0$.
Let $\gamma=m/n, m<n$ and $(m,n)=1$, then $\sigma_1^{\gamma}=\sigma_1^{m/n}=s_1=s_1\left(\cos(2l\pi)+i\sin(2l\pi)\right)$, $l=0,1,2,3,...$ This equation has m roots, $\sigma_{1,l}$ $(l=0,1,...,m-1)$ for σ_1, where

$$\sigma_{1,l}(\alpha,\lambda,d,\mu,\gamma)=s_1^{1/\gamma}\left(\cos\frac{2ln\pi}{m}+i\sin\frac{2ln\pi}{m}\right),\quad l=0,1,2,3,...,m-1. \quad (2.20)$$

Then the maximum values of the real parts among the solutions, $\{\sigma_{1,l}\}$, of equation (2.19) is $\max_l \sigma_{1,l}(\alpha,\lambda,d,\mu,\gamma)=(\max_l s_1(\alpha,\lambda,d,\mu))^{1/\gamma}=\sigma_{1,0}=s_1^{1/\gamma}$. Therefore, if the conditions C_1 to C_4 are satisfied, then the solutions of the system (1.5) are unstable. The conditions C_1 to C_4 are the same as the Turing instability conditions for standard ($\gamma=1$) Reaction Diffusion equations but the growth rate, σ, depends on γ. In terms of the model parameters, the instability conditions at S_2 when $h(\mu)<0$ can be represented in the following form:

$$C_1 \equiv \frac{\alpha^2-4\lambda^2+\alpha\sqrt{\alpha^2-4\lambda^2}}{2\lambda}>0,$$
$$C_2 \equiv -\frac{\alpha^2-2\lambda^3+\alpha\sqrt{\alpha^2-4\lambda^2}}{2\lambda^2}<0,$$
$$C_3 \equiv \frac{2\lambda^3-\alpha d(\alpha+\sqrt{\alpha^2-4\lambda^2})}{2\lambda^2}>0,$$
$$C_4 \equiv \left(\frac{2\lambda^3-d\alpha(\alpha+\sqrt{\alpha^2-4\lambda^2})}{2\lambda^2}\right)^2-4d\left(\frac{\alpha^2-4\lambda^2+\alpha\sqrt{\alpha^2-4\lambda^2}}{2\lambda}\right)>0.$$

As in [17] the instability region (Turing space) can be obtained as a union of two regions $\mathcal{R}_1$ and $\mathcal{R}_2$. Here,

$$\mathcal{R}_1=\{(\lambda,\alpha);\quad 2d\leq\lambda\leq 2,\quad \alpha_{\text{min}}(\lambda)<\alpha<\alpha_{\text{max}}(\lambda,d)\},$$

$$\mathcal{R}_2 = \{(\lambda, \alpha); \quad \lambda > 2, \quad \alpha_{\min}(\lambda) < \alpha < \alpha_{\max}(\lambda, d)\},$$

where $\alpha_{\min}(\lambda) = \begin{cases} 2\lambda, & \text{if } 2d \leq \lambda \leq 2 \\ \dfrac{\lambda^2}{\lambda - 1}, & \text{if } \lambda > 2, \end{cases}$

$$\alpha_{\max}(\lambda, d) = \frac{\lambda^{3/2}\sqrt{(8d^2 + 7d\lambda + 3\lambda^2) - 2\sqrt{2}(2d + \lambda)\sqrt{\lambda(\lambda - d)}}}{d^{1/2}(d + \lambda)}.$$

Next we discuss the effect of the model parameters on the growth and the spatial temporal pattern formation behaviour of the solutions of the model.

3. Results and Discussion

3.1. Critical values of d. It can be shown that in order to satisfy the conditions C_3 and C_4 the condition $d < d_c(\alpha, \lambda)$ should be satisfied. Here

$$d_c(\alpha, \lambda) = \frac{3\,\alpha\,\lambda^3\left(\alpha + \sqrt{\alpha^2 - 4\,\lambda^2}\right) - \mathcal{A}}{\alpha^2\,\left(\alpha^2 - 2\,\lambda^2 + \alpha\,\sqrt{\alpha^2 - 4\,\lambda^2}\right)},$$

$$\mathcal{A} = 4\lambda^3\left[2\,\lambda^2 + (\alpha^2 - 4\lambda^2)^{1/4}\sqrt{(\alpha^2 - \lambda^2)(\alpha^2 - 4\lambda^2)^{1/2} + \alpha^3 - 3\alpha\lambda^2}\right].$$

3.2. Effect of the fractional exponent and the diffusion rate on pattern formation and growth. As time increases the solution of the linearised system (2.17) is dominated by the wave numbers corresponding to the maximum value of growth rate σ.

It can be shown that when $d < d_c$ there exist two values $k = k^{(1)}$ and $k = k^{(2)}$ such that the real part of σ, Re(σ), is positive when $k \in (k^{(1)}, k^{(2)})$. This behaviour is depicted in Figure (1). By these properties we can conclude that when $d < d_c$ and $k \in (k^{(1)}, k^{(2)})$ spatial temporal patterns exist in the model.

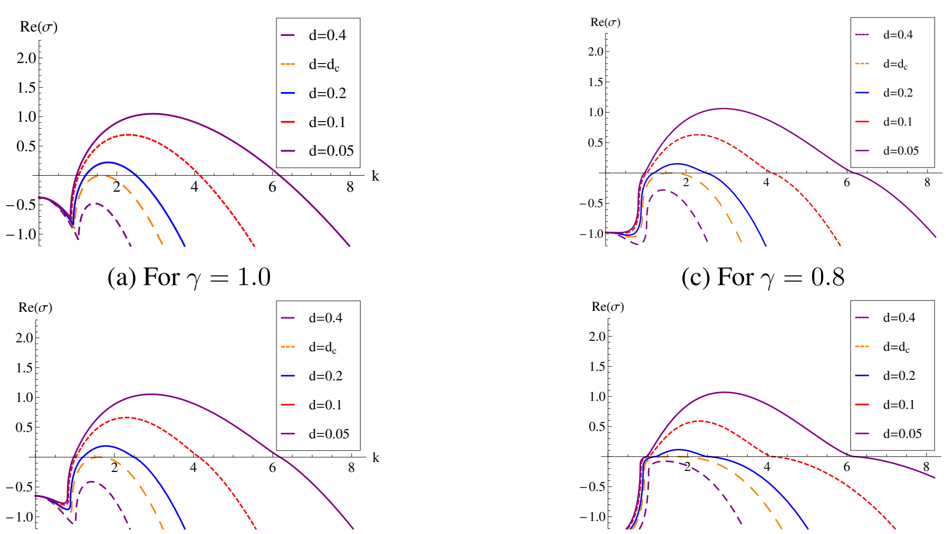

(a) For $\gamma = 1.0$ (c) For $\gamma = 0.8$

(b) For $\gamma = 0.9$ (d) For $\gamma = 0.7$

Figure 1. The variation of Re(σ) against k at different levels of d for particular γ values. The other parameters are set as $\alpha = 4.4$, $\lambda = 2.1$.

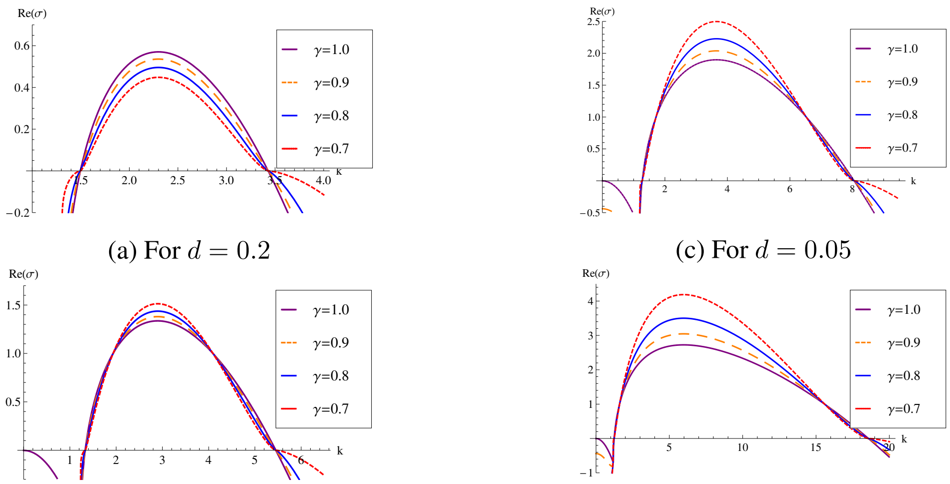

(a) For $d = 0.2$ (c) For $d = 0.05$

(b) For $d = 0.1$ (d) For $d = 0.01$

FIGURE 2. The variation of Re(σ) against k at different levels of γ for particular d values. The other parameters are set as $\alpha = 7.75$, $\lambda = 3.5$.

According to Figure 2 we can conclude that as γ decreases, the maximum value of Re(σ) increases when $k \in (k^{(1)}, k^{(2)})$. Therefore, the growth rate increases as the temporal fractional exponent decreases.

Consider the dispersion relation (2.19). Solving this equation for σ^γ we find $\sigma_{1,2}^{\gamma} = \dfrac{g(\mu) \pm \sqrt{(g(\mu))^2 - 4h(\mu)}}{2}$.

Critical values of σ are given by

$$\frac{d\sigma^\gamma}{d\mu} = 0. \tag{3.21}$$

Solving 3.21 for μ we get two solutions μ_1 and μ_2 given by

$$\mu_1 = k_1^2 = \frac{A_2 + B_2}{2\, d\, (1-d)\, \lambda^2},$$

$$\mu_2 = k_2^2 = \frac{A_2 - B_2}{2\, d\, (1-d)\, \lambda^2},$$

where

$$\begin{array}{rcl} A_2 & = & 2(d+1)\lambda \sqrt{d\lambda \left(\alpha^2 - 2\,\lambda^2 + \alpha\sqrt{\alpha^2 - 4\,\lambda^2}\right)} \text{ and} \\ B_2 & = & \left(\alpha^2 + 2\,\lambda^3 + \alpha\sqrt{\alpha^2 - 4\,\lambda^2}\right). \end{array}.$$

It can be shown that σ is maximized at $\mu = \mu_1$. That is $\sigma_{\max}(\alpha, \lambda, \gamma) = \sigma|_{\mu=\mu_1}$. Also $\sigma_1^\gamma > \sigma_2^\gamma$. Therefore $\sigma_{\max}(\alpha, \lambda, \gamma) = \sigma_1|_{\mu=\mu_1} = \left(\dfrac{g(\mu_1) + \sqrt{(g(\mu_1))^2 - 4h(\mu_1)}}{2}\right)^{1/\gamma}$.

The plots of $\sigma_{\max}$ against α for different levels of γ are shown in Figure (3).

Let $\gamma_1, \gamma_2 \in (0, 1]$ and $\gamma_1 \neq \gamma_2$. Then, it can be shown that the surfaces $\sigma_{\max}(\alpha, \lambda, \gamma_1)$ and $\sigma_{\max}(\alpha, \lambda, \gamma_2)$ intersect on a curve. By simple calculation it can be shown that this curve is given by $g(\mu_1) - h(\mu_1) = 1$. That is on the surface $g(\mu_1) - h(\mu_1) = 1$, the value of $\sigma_{\max}(\alpha, \lambda, \gamma)$ is independent of γ. That is maximum growth rate is independent of γ on the surface $g(\mu_1) - h(\mu_1) = 1$. It can numerically be shown that the equation

$g(\mu_1) - h(\mu_1) = 1$ has four solutions for α at given $\lambda = \lambda_0$ and $d = d_0$. Among these solutions, one is $\alpha_{\max}(\lambda_0, d_0)$ and another lies between $\alpha_{\min}(\lambda_0)$ and $\alpha_{\max}(\lambda_0, d_0)$ and the other two are greater than $\alpha_{\max}$.

That is, for any distinct γ_1 and γ_2, the curves $\sigma_{\max}(\alpha, \lambda_0, d_0, \gamma_1)$ and $\sigma_{\max}(\alpha, \lambda_0, d_0, \gamma_2)$ intersect at the fixed point $\alpha = \alpha_0 \in (\alpha_{\min}(\lambda_0), \alpha_{max}(\lambda_0, d_0))$. Figure (3) depicts this behaviour. Hence at the position $(\lambda_0, d_0, \alpha_0)$ the maximum growth rate is independent of γ.

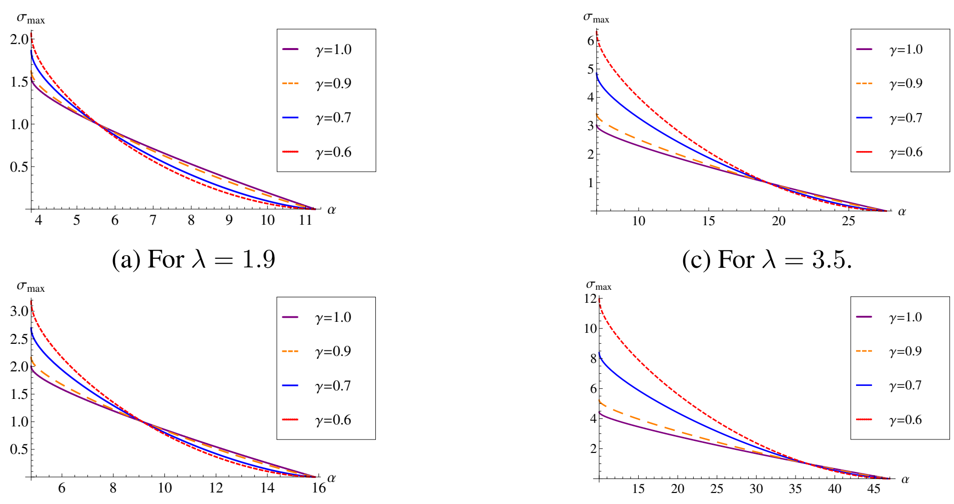

(a) For $\lambda = 1.9$ (c) For $\lambda = 3.5$.

(b) For $\lambda = 2.4$ (d) For $\lambda = 5.0$

FIGURE 3. The variation of $\sigma_{\max}$ against α at different levels of γ for $d = 0.01$.

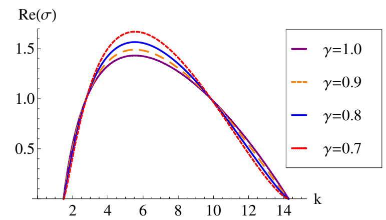

(a) For $\alpha = \alpha_{\gamma\text{free}} - 2$

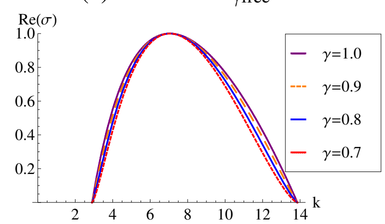

(b) For $\alpha = \alpha_{\gamma\text{free}}$

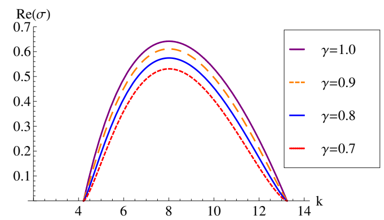

(c) For $\alpha = \alpha_{\gamma\text{free}} + 2$

FIGURE 4. The variation of Re(σ) against k. (a) $\alpha_{\min}(\lambda, d) < \alpha_{\gamma\text{free}}(\lambda, d) - 2 < \alpha_{\gamma\text{free}}(\lambda, d)$ (b) $\alpha = \alpha_{\gamma\text{free}}(\lambda, d)$ (c) $\alpha_{\gamma\text{free}}(\lambda, d) < \alpha_{\gamma\text{free}}(\lambda, d) + 2 < \alpha_{\max}(\lambda, d)$. Here $d = 0.01$, $\lambda = 2.1$ and $\alpha_{\gamma\text{free}}(2.1, 0.01) = 6.89566$.

Let $\alpha = \alpha_{\gamma\text{free}}(\lambda, d) \in (\alpha_{\min}(\lambda), \alpha_{\max}(\lambda, d))$ be the positive solution for α of the equation $g(\mu_1) - h(\mu_1) = 1$ for given λ and d. We can show that

$$\alpha_{\gamma\text{free}} = \frac{\lambda\sqrt{(3\lambda+1)\left[d(5d+4\lambda-4)+(\lambda-1)^2\right]-\mathcal{A}_1}}{d^{1/2}(2d+\lambda-1)}.$$

Here $\mathcal{A}_1 = 2d^3 + 2\sqrt{2}(3d+\lambda-1)(d+\lambda-1)\sqrt{\lambda(\lambda+1-2d)}$.
Also, let $d = d_{\gamma\text{free}}(\alpha, \lambda)$ be the solution for d of the equation $g(\mu_1) - h(\mu_1) = 1$ for a given α and λ. However, it is impossible to solve the equation $g(\mu_1) - h(\mu_1) = 1$ explicitly for d. But it can be solved for d numerically for a given λ.

The curves $\alpha = \alpha_{\min}(\lambda)$, $\alpha = \alpha_{\gamma\text{free}}(\lambda, d)$ and $\alpha = \alpha_{\max}(\lambda, d)$ against λ at $d = 0.01$ are shown in Figure (5)(a) and numerically evaluated $d = d_{\gamma\text{free}}(\lambda, \alpha)$ against α for different levels of λ are shown in Figure (5)(b).

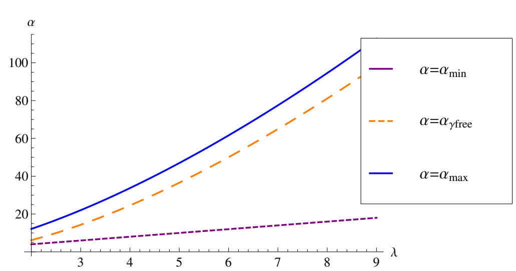

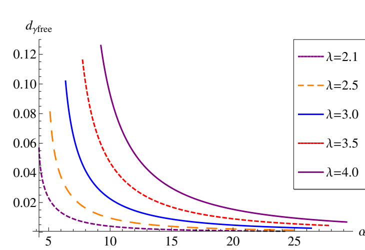

(a) (b)

FIGURE 5. (a)The variation of $\alpha_{\min}$, $\alpha_{\gamma\text{free}}$ and $\alpha_{\max}$ against λ at $d = 0.01$, (b) The variation of $d_{\gamma\text{free}}$ against α at different levels of λ.

It is clear that $\sigma_{\max}(\alpha,\lambda)$ is maximized at $\alpha=\alpha_{\min}(\lambda)$. The wavelength corresponding to the maximum growth rate is given by $\omega_{\max}=2\pi/k_1$. The wave number $n_{\max}$ corresponding to the maximum growth rate, $\sigma_{\max}$, on the domain $[0,L]$ is given by $n_{\max}=k_1L/\pi$. The plot of $n_{\max}$ against α for different levels of d are shown in Figure (6). We can observe that for fixed λ and d the value $n_{\max}$ increases as α increases. In addition, as d decreases $n_{\max}$ increases.

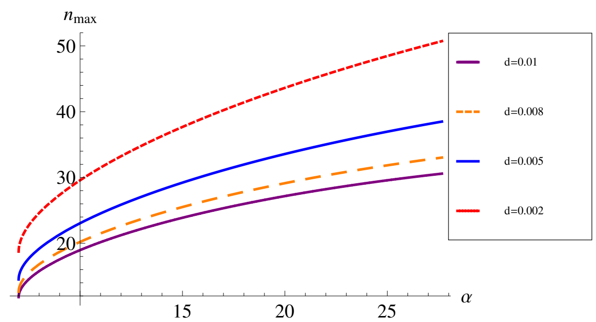

FIGURE 6. The variation of $n_{\max}$ against α for different levels of d when $\lambda=3.5$.

3.3. **Numerical results.** The system of ODEs (system(2.8)) with initial conditions $\mathbf{u}^0$ and $\mathbf{v}^0$ was simulated on $\Omega=[0,L]\subset\mathbb{R}$ and on $\Omega=[0,L]\times[0,L]\subset\mathbb{R}^2$ on the time interval $[0,T]$ using the numerical schemes given by equation (2.13) explained in section 2.1. Here $\mathbf{u}^0$ and $\mathbf{v}^0$ are the spatial discretisations of $u(\mathbf{x},0)$ and $v(\mathbf{x},0)$, respectively, where $\mathbf{x}\in\Omega$.

3.3.1. *Numerical solutions in one spatial dimension.* The system (2.8) was solved when $L=8$ and

$$\begin{aligned} u(x,0) &= \quad u_{02}, \quad x\in\Omega, \\ v(x,0) &= \begin{cases} v_{02}+v_{02}\dfrac{\text{Rand}[0,1]}{10}, & x\in\omega \\ 0, & x\in\Omega\backslash\omega. \end{cases} \end{aligned} \tag{3.22}$$

Here $\omega=\left(\dfrac{L}{2}-\dfrac{5L}{100},\dfrac{L}{2}+\dfrac{5L}{100}\right)$. Numerical solutions at three time levels obtained by proposed numerical scheme are shown in Figure (7). In these simulations $L=8$, $T=40$, and the spatial and time grid sizes are $\Delta x=0.05$ and $\Delta t=0.005$, respectively.

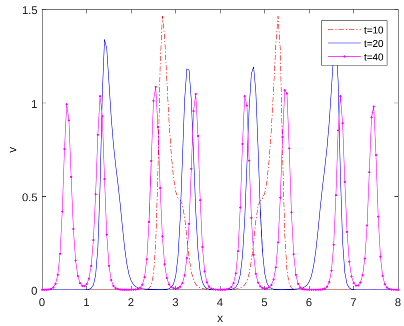

FIGURE 7. v component of the numerical solutions of (1.5) for the parameter values $\gamma = 0.9$, $\lambda = 3.5$, $\alpha = 7.75$, $d = 0.01$ at time levels $t = 10$, $t = 20$ and $t = 40$.

Figure (8) depicts how the relative error (equation (2.14))of the last iteration at each time step of the fully implicit scheme is maintained by the tolerance of the above numerical simulations. As the relative error maintains the tolerance properly, we can conclude that the numerical solutions of the Fully Implicit scheme converge to the solution of the considered fractional reaction diffusion system.

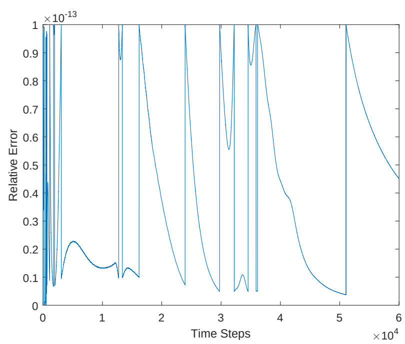

(a) $\gamma = 1$

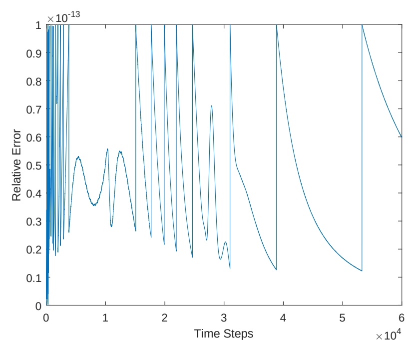

(c) $\gamma = 0.8$

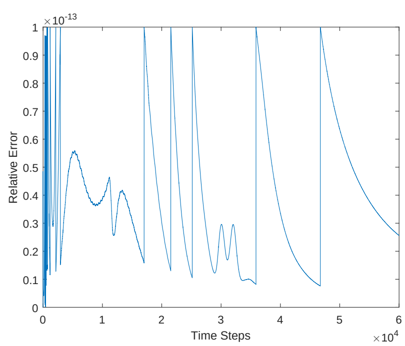

(b) $\gamma = 0.9$

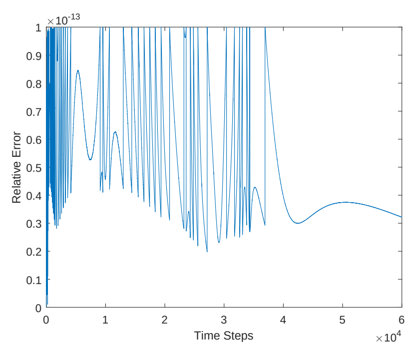

(d) $\gamma = 0.7$

FIGURE 8. The relative error of the fully implicit scheme (relative error of the last iteration at each time step) when the time step size is 0.001.

3.3.2. *Numerical solution in two spatial dimension.* The system (2.8) is solved numerically on the 2D domain with $L = 4$ and initial conditions:

$$\begin{aligned} u(x,y,0) = &\ \ u_{02}, \quad (x,y) \in \Omega, \\ v(x,y,0) = &\begin{cases} v_{02} + v_{02}\dfrac{\text{Rand}[0,1]}{10}, & (x,y) \in \omega \\ 0, & (x,y) \in \Omega \backslash \omega. \end{cases} \end{aligned} \tag{3.23}$$

Here $\omega = \left\{ (x,y) \in \Omega, \quad \dfrac{L}{2} - \dfrac{5L}{100} < x < \dfrac{L}{2} + \dfrac{5L}{100}, \quad \dfrac{L}{2} - \dfrac{5L}{100} < y < \dfrac{L}{2} + \dfrac{5L}{100} \right\}.$

Isosurfaces of the numerically evaluated $v(x,y,t)$ using the fully implicit scheme are shown in Figures (9). In these simulations the spatial and time grid sizes are $\Delta x = 0.05$ and $\Delta t = 0.005$, respectively.

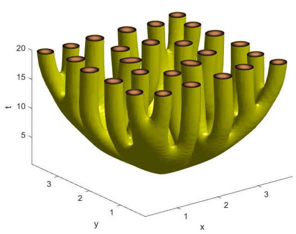

(a) For $\gamma = 1.0$.

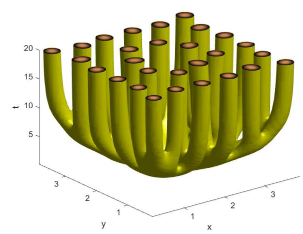

(c) For $\gamma = 0.8$.

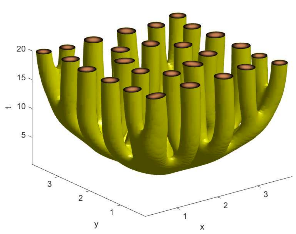

(b) For $\gamma = 0.9$.

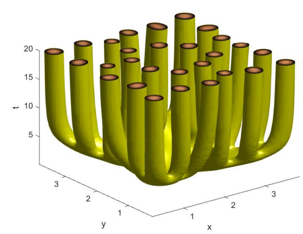

(d) For $\gamma = 0.7$.

FIGURE 9. Isosurfaces of numerical solutions $v(x,y,t)$ at different values of γ for the parameter values $\lambda = 3.5$, $\alpha = 7.75$, $d = 0.01$.

According to Figure (9) the number of branches of the spatial-temporal patterns does not depend on γ. That is, this numerical result agree with the property that n_{max} is independent of γ. Also, we can observe that the time spent to make branches decreases as γ decreases. This result agree with the theoretically derived result that when $\alpha < \alpha_{\gamma\text{free}}(\lambda, d)$ the maximum growth rate, σ_{max} increases as γ decreases.

Figure (10) shows the variation of patterns with diffusion rate d when other parameters and the fractional order are fixed. We observed that as d decreases the heterogeneity of the spatial-temporal patterns increases. This result agree with the effect of the d on pattern formation shown in Figure (6).

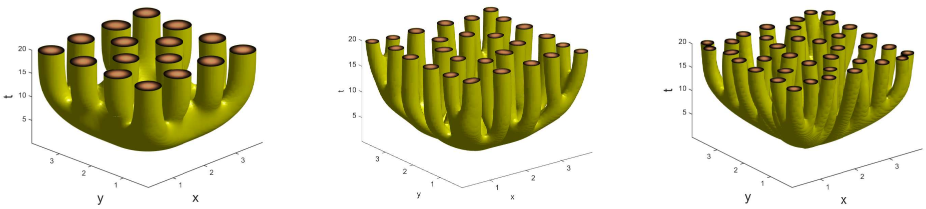

(a) For $d = 0.02$. (b) For $d = 0.01$. (c) For $d = 0.005$.

FIGURE 10. Isosurfaces of numerical solutions $v(x, y, t)$ at different levels of d for the parameter values $\lambda = 3.5$, $\alpha = 7.75$ and $\gamma = 0.9$.

4. Conclusions

We can draw a number of conclusions from our analysis and numerical simulations. The real part of the growth rate σ, Re(σ), increases as d decreases from d_c. Also the wave mode corresponds to maximum growth rate and the range of unstable wave modes increases as d decreases from d_c. These observations imply that as d decreases from d_c, the growth rate increases and the heterogeneity of the spatial structures formed by the solutions of the model increases.

For a fixed d, the range of unstable wave modes (the range of k) does not depend on γ whereas Re(σ) does. In addition, the wave mode corresponding to the maximum growth rate does not depend on γ when other parameters are fixed.

There exist a surface $\phi(\alpha, \lambda, d) = g(\mu_1) - h(\mu_1) - 1 = 0$ on which maximum growth rate is independent of γ. In other words, the spatial temporal pattern formation behaviour of the model is independent of the time fractional exponent at a point (say $(\alpha_{\gamma\text{free}}, \lambda_{\gamma\text{free}}, d_{\gamma\text{free}})$) on the surface given by $\phi(\alpha, \lambda, d) = 0$.

As α increases from α_{min} to α_{max} by keeping other parameters fixed, the value of n_{max} increases. Also, n_{max} increases as d decreases. This implies that the heterogeneity of the spatial patterns generated by the solutions increases as α increases and d decreases when other parameters are fixed. In addition, the spatial heterogeneity does not depend on the value of γ whereas the growth rate does.

References

[1] I. Podlubny, Fractional differential equations: an introduction to fractional derivatives, fractional differential equations, to methods of their solution and some of their applications, Academic press, 1998.

[2] S.Z. Rida, A. M. A. El-Sayed and A. A. M. Arafa, On the solutions of time-fractional reaction–diffusion equations,*Communications in Nonlinear Science and Numerical Simulation*, Vol. 15, No. 12, pp. 3847–3854, 2010.

[3] R. Scherer, S. L. Kalla, Y. Tang and J. Huang, The Grünwald-Letnikov method for fractional differential equations *Computers & Mathematics with Applications*, Vol. 62, No. 3, pp. 902–917. 2011.

[4] Q. Yu, F. Liu, V. Anh and I. Turner, Solving linear and non-linear space-time fractional reaction-diffusion equations by the Adomian decomposition method, *International journal for numerical methods in engineering*, Vol. 74, No. 1, pp. 138-158. 2008.

[5] Q. Yang, T. Moroney, K. Burrage and I. Turner and F. Liu, Novel numerical methods for time-space fractional reaction diffusion equations in two dimensions, *ANZIAM Journal*, vol. 52, pp. 395-409, 2010.

[6] S. B. Yuste and L. Acedo, An explicit finite difference method and a new von Neumann-type stability analysis for fractional diffusion equations, *SIAM Journal on Numerical Analysis*, vol. 42, No. 5, pp. 1862-1874, 2005.

[7] P. Zhuang and F. Liu, Implicit difference approximation for the time fractional diffusion equation *Journal of Applied Mathematics and Computing*, vol. 22, No. 3, pp. 87-99, 2006.

[8] Y. Xu and Z. He, The short memory principle for solving Abel differential equation of fractional order, *Computers & Mathematics with Applications*, Vol. 62, No. 12, pp. 4796-4805, 2011.

[9] W. Deng and C. Li, *Numerical schemes for fractional ordinary differential equations*,2012, INTECH Open Access Publisher.

[10] C. M. Chen, F. Liu, V. Anh and I. Turner, Numerical methods for solving a two-dimensional variable-order anomalous subdiffusion equation *Mathematics of Computation*, Vol. 81, No. 277, pp. 345-366, 2012.

[11] B. Baeumer, M. Kovács and M. M. Meerschaert, Numerical solutions for fractional reaction–diffusion equations, *Computers & Mathematics with Applications*, Vol. 55, No. 10, pp. 2212-2226, 2008.

[12] Y. Lin and C. Xu, Finite difference/spectral approximations for the time-fractional diffusion equation, *Journal of Computational Physics*, Vol. 225, No. 2, pp. 1533-1552, 2007,

[13] F. Liu, C. Yang and K. Burrage, Numerical method and analytical technique of the modified anomalous subdiffusion equation with a nonlinear source term, *Journal of Computational and Applied Mathematics*, Vol 231, No. 1, pp. 160–176, 2009.

[14] V. Gafiychuk, B. Datsko and V. Meleshko, Mathematical modeling of time fractional reaction–diffusion systems, *Journal of Computational and Applied Mathematics*, Vol. 220, No. 1, pp. 215-225, 2008.

[15] B. Y. Datsko and V. V. Gafiychuk, *Analysis of instabilities and pattern formation in time fractional reaction-diffusion systems*,
arXiv preprint arXiv:0912.1500, 2009.

[16] T. A. M. Langlands, B. I. Henry and S. L. Wearne, Turing pattern formation with fractional diffusion and fractional reactions, *Journal of Physics: Condensed Matter*, Vol. 19, No. 6, pp. 1-20, 2007.

[17] L. W. Somathilake and K. Burrage, A space-fractional-reaction-diffusion model for pattern formation in coral reefs, *Cogent Mathematics & Statistics*, Vol. 5, pp. 1-21, 2018.

[18] C. M. Chen, F. Liu, I. Turner and V. O. Anh, A Fourier method for the fractional diffusion equation describing sub-diffusion, *Journal of Computational Physics*, Vol. 227, No. 2, pp. 886–897, 2007.

[19] C. M. Chen and F. Liu, A numerical approximation method for solving a three-dimensional space Galilei invariant fractional advection-diffusion equation, *Journal of Applied Mathematics and Computing*, Vol. 30, No.1, pp. 219–236, 2009.

[20] İ. Karatay, Ş. R. Bayramoğlu and A. Şahin, Implicit difference approximation for the time fractional heat equation with the nonlocal condition, *Applied Numerical Mathematics*, Vol. 61, No. 12, pp. 1281-1288, 2011.

L. W. SOMATHILAKE

DEPARTMENT OF MATHEMATICS, FACULTY OF SCIENCE, UNIVERSITY OF RUHUNA, MATARA, SRI LANKA.

E-mail address: sthilake@maths.ruh.ac.lk, lwsoma@gmail.com

K. BURRAGE

SCHOOL OF MATHEMATICAL SCIENCES, QUEENSLAND UNIVERSITY OF TECHNOLOGY, BRISBANE, AUSTRALIA.

VISITING PROFESSOR IN COMPUTER SCIENCE, DEPARTMENT OF COMPUTER SCIENCE, UNIVERSITY OF OXFORD, WOLFSON BUILDING, PARKS ROAD, OXFORD, OX1 3QD, UK.

CHIEF INVESTIGATOR, THE ARC CENTRE OF EXCELLENCE ACEMS, AUSTRALIA.

E-mail address: kevin.burrage@qut.edu.au